Lateral Subunit Coupling Determines Intermediate Filament Mechanics

Charlotta Lorenz,[1] Johanna Forsting,[1] Anna V. Schepers,[1] Julia Kraxner,[1] Susanne Bauch,[1] Hannes Witt,[2,3] Stefan Klumpp,[4] and Sarah Köster[1,*]

[1]Institute for X-Ray Physics, University of Göttingen, Friedrich-Hund-Platz 1, 37077 Göttingen, Germany
[2]Institute for Organic and Biomolecular Chemistry, University of Göttingen, Tammanstraße 2, 37077 Göttingen, Germany
[3]Max Planck Institute for Dynamics and Self-Organization, Am Faßberg 7, 37077 Göttingen
[4]Institute for Dynamics of Complex Systems, University of Göttingen, Friedrich-Hund-Platz 1, 37077 Göttingen, Germany

(Received 14 May 2019; published 29 October 2019)

The cytoskeleton is a composite network of three types of protein filaments, among which intermediate filaments (IFs) are the most extensible ones. Two very important IFs are keratin and vimentin, which have similar molecular architectures but different mechanical behaviors. Here we compare the mechanical response of single keratin and vimentin filaments using optical tweezers. We show that the mechanics of vimentin strongly depends on the ionic strength of the buffer and that its force-strain curve suggests a high degree of cooperativity between subunits. Indeed, a computational model indicates that in contrast to keratin, vimentin is characterized by strong lateral subunit coupling of its charged monomers during unfolding of α helices. We conclude that cells can tune their mechanics by differential use of keratin versus vimentin.

DOI: 10.1103/PhysRevLett.123.188102

The cytoskeleton is composed of three types of biopolymers—actin filaments, microtubules, and intermediate filaments (IFs)—which, along with cross-linkers and motor proteins, form a dense network in the cell [1] and determine its mechanical properties. Microtubules and actin filaments are conserved across different cell types and organisms. By contrast, IFs are expressed in a cell-type specific manner [2–4]: For example, keratins are predominantly expressed in epithelial cells and vimentin in cells of mesenchymal origin. It has been shown that vimentin deprived cells are less mechanically stable and migrate more slowly [5], whereas cells lacking keratin are softer and more deformable [6,7]. These differences are likely to play an important role during the endothelial-to-mesenchymal transition, for example, in embryogenesis, wound healing and cancer metastasis, when cells upregulate vimentin expression and downregulate keratin expression [4,8–10]. We hypothesize that keratin and vimentin IFs have different mechanical properties already at the single filament level. It has been demonstrated previously that single vimentin IFs exhibit a pronounced extensibility of up to 4.5 times their original length [11–13] and a high flexibility [14–16], and can dissipate up to 80% of the input energy when stretched and relaxed [17]. Keratin has so far been primarily studied in the context of bundles, for example, in hagfish slime threads [18], wool fibers [19], and hard α-keratin fibers [20]. However, data from single filaments are needed to decouple the mechanics resulting from the bundle or network structure, i.e., the interfilament interactions, from the single filament mechanics.

IF mechanics are closely linked to their molecular architecture [13,17,21]. The monomer consists of a "rod" domain including three α helices, which are connected by linkers and flanked by intrinsically disordered head and tail regions [Figs. 1(a) and 1(b)] [22]. Despite differing amino acid sequences, all cytoskeletal IFs share this monomer structure, as well as the particular assembly pathway: Two monomers form a parallel dimer, two dimers an antiparallel, half-staggered tetramer, and tetramers eventually form unit-length filaments (ULFs) with a length of about 60 nm [22]. This lateral assembly is followed by longitudinal annealing of ULFs resulting in μm-long filaments. One important difference between keratin and vimentin IFs is the average number of tetramers per filament cross section of four and eight, respectively [2]. During stretching of these filaments, the α helices open into an unfolded state leading to a contour length change [17,23,24].

Here, we study the mechanical behavior of single keratin and vimentin IFs under load by stretching them with optical traps (OTs) [13,17]. It is well known that keratin and vimentin are held together mainly by hydrophobic and electrostatic interactions. Therefore, we use two distinctly different buffer conditions with high or low ionic strength, respectively, to tune the electrostatic interactions. We find that ionic strength impacts IF mechanics, which we explain by stronger lateral coupling in vimentin subunits than in keratin subunits, corroborated by data from atomic force microscopy (AFM). The experimental data from OT are modeled and quantitatively fitted by a Monte Carlo (MC) simulation based on the IF structure [17]. From the fit, we obtain the free energy difference between the folded α helix and the unfolded state, and the α-helical stiffness.

Proteins are recombinantly expressed [25], labeled and reconstituted to tetrameric form as described in the

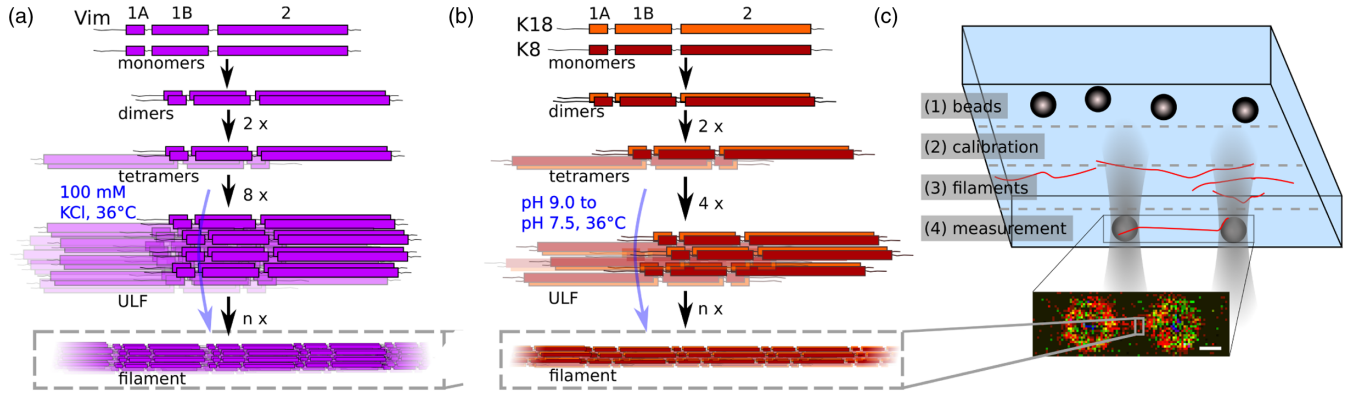

FIG. 1. (a,b) Assembly pathway of vimentin (Vim) and keratin (K8, K18) IFs, respectively. The monomers consist of three α-helical regions (1A, 1B, 2) connected by two linkers and flanked by intrinsically unstructured regions, and form extended IFs in a strictly hierarchical manner. (c) Top: Schematic of the microfluidic device used for measurements with the OT. Bottom: Confocal image of a fluorescently labeled keratin IF captured between 4.42-μm-diameter beads; the scale bar is 2 μm.

Supplemental Material (SM) [26]. Keratin is assembled at 0.1 mg/mL by dialysis into a low ionic strength buffer, a standard keratin buffer (LB: 10 mM TRIS, pH 7.5) [2,27–31], and vimentin at a protein concentration of 0.2 mg/mL into a physiological, high ionic strength buffer (HB: 100 mM KCl, 2 mM phosphate buffer, pH 7.5) [27–29,32–34], both at 36 °C overnight. In both cases, about 4% of all monomers are labeled fluorescently with ATTO647N.

For OT measurements, the assembled keratin and vimentin filaments are diluted 1:70 and 1:100, respectively, with the corresponding assembly buffer. The OT trap setup (LUMICKS, Amsterdam, Netherlands) is equipped with a confocal fluorescence microscope and a microfluidic device as sketched in Fig. 1(c). Polystyrene beads (Kisker Biotech, Steinfurt, Germany) are maleimide coated [35] to allow for covalent binding to the IFs via cysteins. The beads are diluted with the assembly buffer of the respective studied protein, which is also used as a buffer in the calibration channel. The buffer in channel (4) is either LB or HB, and each IF is studied in both buffers.

Before each measurement, two beads are captured with the OT in channel (1), and the trap stiffness is calibrated via their thermal noise spectrum in channel (2). IFs are attached to the beads in channel (3), and it is ensured by fluorescence microscopy that only one IF is bound to the beads. The traps with the IF are moved to channel (4) and incubated for 30 s, unless the measurement is intended to take place in the assembly buffer of the respective IF protein. One OT is moved with speeds between 0.3 μm/s and 2.5 μm/s to stretch the IF in channel (4). The force exerted on the IF by the OT as well as the bead positions are recorded.

IF heights are measured with a commercial AFM (Infinity, Oxford Instruments Asylum Research, Santa Barbara, CA, USA). IFs are incubated for 30 s in the buffer of interest, fixed with 0.125% glutaraldehyde and imaged on a piece of silicon wafer (Crystec, Berlin, Germany) in buffer. Cantilevers (MLCT, Bruker, Billerica, MA, USA) are calibrated via their thermal noise spectrum.

From the OT data, the strain $\varepsilon = L/L_0 - 1$ is calculated [17] using the measured IF length L and the IF length L_0 at 5 pN. The individual and average force-strain curves of single keratin and vimentin IFs in the two buffer conditions are shown in Figs. 2(a) and 2(b). The averages are calculated by averaging both force and strain data (see SM, including Figs. S1 and S2 [26]).

In contrast to keratin, the force-strain behavior of vimentin filaments significantly depends on the ionic strength of the buffer as Fig. 2 shows. Figure S6 in the SM [26] shows the same data, however, grouped according to filament type. In LB, the force-strain behavior of keratin and vimentin is similar and can be divided into three regimes [13,17]: There is an elastic regime for low strains caused by the elastic behavior of α helices [13,21,36,37]. A less steep regime for strains between 0.2 and 0.8 arises from the stepwise opening of α helices during elongation [21,23]. The filaments stiffen again for high strains since most α helices are unfolded and the resulting structure is stretched [21]. The slopes for low strains (in the range of 0.015–0.1 or 0.015–0.15, depending on the linear regime) are, on average, slightly higher for vimentin compared to keratin filaments [Figs. 2(c) and 2(d)], which can be partially explained by the doubled number of monomers per cross section in vimentin IFs. In summary, for keratin and vimentin filaments, there is a small initial slope and no considerably decreased slope for intermediate strains in LB, similar to the previously observed stress-strain behavior of IF bundles [18] [Fig. 2(a)]. A detailed analysis of the slope behavior for intermediate strains is included in Fig. S3 in the SM [26]. By contrast, the two filament types behave differently in HB [Fig. 2(b)]. For keratin filaments, there is no clear separation between the regimes. Vimentin filaments, however, show a high initial slope and a plateaulike region, which indicates some degree of

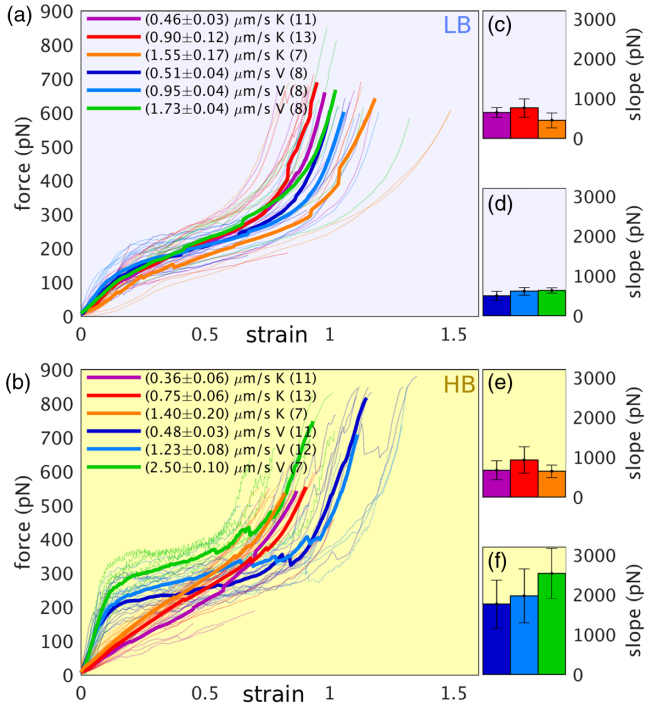

FIG. 2. (a,b) Force-strain curves for keratin (K, warm colors) and vimentin (V, cold colors) in (a) LB (blue background) and (b) HB (yellow background) measured with the OT. The curves from single IFs (thin lines) for different loading rates (see color code) are averaged (thick lines). The number of measurements for each condition is included in parentheses in the legend. (c)–(e) Initial slopes with standard deviations obtained from linear fits in the low strain regime of (c) keratin in LB, (d) vimentin in LB, (e) keratin in HB, and (f) vimentin in HB.

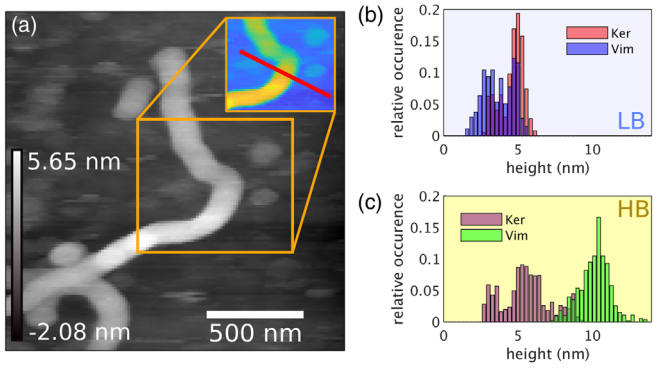

FIG. 3. (a) Typical AFM image. The inset shows the processed AFM image in MATLAB used to extract the height profile (red line). (b,c) Histogram of keratin and vimentin filament heights measured with AFM in (b) LB and (c) HB.

cooperativity as will be discussed further below. Both proteins are initially stiffer in HB [Figs. 2(e) and 2(f)].

The different curve shapes for keratin and vimentin filaments also result in a higher input energy E for vimentin than for keratin filaments in HB. Note that E_{XY} is calculated by integrating the force-strain curves up to a force of 500 pN of protein X in buffer Y. In LB, the ratio of the input energies E_{VL}/E_{KL} is 1.02 ± 0.18, whereas in HB, vimentin filaments take up about 53% more energy ($E_{VH}/E_{KH} = 1.53 \pm 0.23$), as shown in Fig. S4(a) in the SM [26].

To understand these data, we take a closer look at the molecular properties of keratin and vimentin. Vimentin carries 19 e/monomer, keratin 8.5 e/monomer. HB has an ionic strength about 20 times higher than LB. The additional ions allow for a closer arrangement of the subunits in the filament since they screen the negative charges and decrease the electrostatic repulsion of the subunits within the filament [38,39]. These additional attractions need to be overcome when the filament is stretched so that the filaments appear initially stiffer in HB. Since vimentin IFs are more negatively charged, they are affected more strongly by a change in the ionic strength of the buffer (see Fig. S6 in the SM [26]). Keratin monomers are 1.5 times more hydrophobic [40] than vimentin monomers, so they attract each other more strongly, independent of the ionic strength of the surrounding buffer. Therefore, we can attribute the increased initial stiffening and the pronounced slope change of the force-strain curve of vimentin filaments in HB to a stronger attraction and a higher lateral coupling strength between the subunits. The higher initial slope and the overall different curve shape also lead to a larger input energy as reported above.

To test this hypothesis, we measure the height of keratin IFs and vimentin IFs in both LB and HB by AFM. The attraction between the substrate and the IF flattens the originally circular cross section of the filament [11,15]. However, a stronger attraction between the filament subunits prevents this effect. IFs in the AFM images are tracked, and the height is extracted from the data as described in the SM [26]. A typical AFM image is shown in Fig. 3(a), and the filament heights agree with the literature [2,41]. The average height for keratin IFs increases from LB to HB by a factor of 1.2 ± 0.4, and the height of vimentin IFs increases by a factor of 2.6 ± 0.9 [Figs. 3(b) and 3(c)]. This supports our hypothesis that HB enhances the attractions between single subunits more strongly in vimentin filaments.

To understand why the lateral coupling in keratin and vimentin IFs has a different effect on the mechanical properties, we model keratin and vimentin IFs based on Refs. [17,42,43]: Each monomer is described as a spring in series with an element that can elongate under tension [Figs. 4(a) and 4(b)]. The spring corresponds to the elastic behavior of an α helix for low forces. The energy difference between the α and unfolded state u is ΔG. Before stretching, N_P monomers are connected in parallel, in order to present a ULF ($N_P = 16$ for keratin, $N_P = 32$ for vimentin). To model a filament, 100 of these ULFs are connected in series by springs. With respect to the elongation of the filament, two variants of the model are

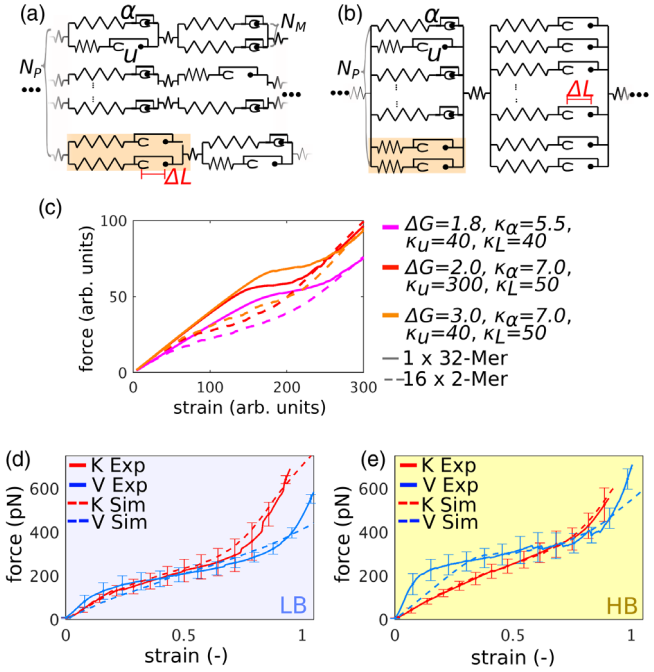

FIG. 4. (a) Model for uncoupled dimers as subunits, case (1), and (b) model for coupled dimers as subunits, case (2). If one subunit is in the unfolded state in case (1), this leads to an elongation by ΔL, whereas in case (2) all monomers have to be in the unfolded state for elongation (orange: elements discussed in the text). (c) Comparison of simulation results for the same parameter sets (see color code in legend) for the uncoupled model (dashed lines) and the coupled model (solid lines), $\Delta L = 1$. (d,e) Measured and simulated force-strain curves (solid and dashed lines, respectively) for keratin (K) and vimentin (V) in (d) LB and (e) HB for the intermediate loading rate shown in Fig. 2.

simulated: In the first (uncoupled) case (1), the filament elongates, when all monomers in one subunit are in the unfolded state [Fig. 4(a)]. In the second (coupled) case (2), the filament elongates, when all monomers of one ULF are in the unfolded state [Fig. 4(b)] [17]. Thus, case (1) supports the idea of protofilaments which can slide past each other [11,44–47].

The coupled and uncoupled extensions differ in how the force ϕ is shared among the monomers M and thus in the force dependence of the transition rates $r^{\alpha\to u}_{A_{j,m}}$ from the α to the unfolded state (see the SM [26]). The transition rate has the general form

$$r^{\alpha\to u}_{A_{j,m}} = A_{j,m} r^{\alpha\to u}_0 \exp\left(\frac{\theta\phi}{M}\right) \tag{1}$$

with the number of monomers $A_{j,m}$ in the α state of the m th subunit in the j th ULF, the zero-force reaction rate from a monomer in the α to the unfolded state $r^{\alpha\to u}_0$, and the load distribution factor θ [48,49]. In the uncoupled case, the force is shared equally among the subunits and within a subunit among the monomers, $M = N_C A_{j,m}$, while in the coupled case, the force is shared equally among all monomers of the ULF, $M = \sum_{m=1}^{N_C} A_{j,m}$ (with the number of laterally associated subunits N_C).

The two different assumptions for elongation lead to a fundamentally different force-strain behavior: In case (1), the data are "s shaped" since the laterally associated α helices in the subunits can open independently at a certain minimum force. In case (2), the initial slope increases and the plateaulike part evolves because a higher minimum force is needed to open the laterally coupled α helices in a cascading manner, which is also observed by Erdmann and Schwarz [43] for a system that resembles one vimentin ULF in HB in our model [50]. Figure 4(c) shows that the same parameter sets for the coupled or uncoupled case, respectively, lead to a qualitatively different behavior. We observe a high initial slope and a reduced slope for intermediate strains only for vimentin filaments in HB; thus, we model them with case (2) [13,17]. For keratin filaments in HB and vimentin and keratin filaments in LB, we assume case (1), which corresponds to an uncoupled filament elongation. We fit the simulation data to the experimental data using MATLAB [Figs. 4(d) and 4(e)]. The simulations agree well with the experimental force-strain curves for keratin filaments in LB and HB and for vimentin filaments in LB; for vimentin filaments in HB, the experiment exhibits a higher initial slope than expected from the simulation. In both buffers, ΔG, as extracted from the fit parameters, lies around 0.3 or 0.6 $k_B T$ per amino acid for keratin or vimentin, respectively, and agrees with theoretical results for short peptides from the literature [52–54]. This indicates that the energy stored in a single α helix does not depend on the ion concentration, in contrast to the lateral coupling strength between the α helices. We also determine the α-helical stiffness of about 0.6–3.4 pN/nm from the simulation parameters in agreement with the literature [13,55,56] as shown in Fig. S4(b) in the SM [26].

Our data from OT, AFM, and MC simulations strongly indicate that the lateral coupling in vimentin filaments induced by additional cations is so strong that all parallel α helices in one ULF have to unfold for a length change, whereas in keratin filaments the filament elongates in any condition as soon as one subunit is in the unfolded configuration. We assume that three main differences in the molecular properties of the two IFs contribute: (i) electrostatics, (ii) hydrophobicity, and (iii) compaction. Aspects (i) and (ii) have been discussed above. Concerning aspect (iii), in contrast to keratin, vimentin IFs compact after elongation [57,58]. This is due to charged amino acids in linker L1 and in coil 1B that attract oppositely charged amino acids in linker L12 from a neighboring tetramer [58,59]. Therefore, compaction can additionally increase the lateral coupling strength in vimentin IFs. Keratin IFs do not compact [60] and also do not exhibit the same charge pattern that all compacting IFs have in common [61] (see Table. II in the SM [26]). Note that it is not the different

number of monomers per cross section in keratin and vimentin that causes the different behavior in HB, as an uncoupled filament with 16 monomers in the MC simulation does not exhibit a high initial slope nor a clear change in slope for intermediate strains (see Fig. S5 in the SM [26]).

To conclude, our experiments substantiate the idea that cells can fine-tune their ability to absorb large amounts of energy to protect the cell from mechanical damage by the expression of different IFs. It should be noted that the ionic environment inside a cell is more complex than what has been used in our experiments, including divalent ions which promote IF bundling [38,62,63]. Depending on the surrounding ion concentration, vimentin filaments stiffen and absorb more energy than keratin filaments. An MC simulation based on assumptions about the molecular structure of both IFs shows that a stronger lateral coupling of the vimentin subunits is the cause for this behavior.

We thank I. Mey for support with the AFM measurements and data analysis. We are grateful for fruitful discussions with and technical support by H. Herrmann, A. Janshoff, U.S. Schwarz, J. Kayser, N. Mücke, U. Rölleke, and P. Rauch. The work was financially supported by the European Research Council (ERC, Grant No. CoG 724932) and the Studienstiftung des deutschen Volkes e.V.

*sarah.koester@phys.uni-goettingen.de

[1] F. Huber, A. Boire, M. P. López, and G. H. Koenderink, Curr. Opin. Cell Biol. **32**, 39 (2015).
[2] H. Herrmann, M. Häner, M. Brettel, N. O. Ku, and U. Aebi, J. Mol. Biol. **286**, 1403 (1999).
[3] H. Herrmann, M. Hesse, M. Reichenzeller, U. Aebi, and T. M Magin, Int. Rev. Cytol. **223**, 83 (2003).
[4] J. Block, V. Schroeder, P. Pawelzyk, N. Willenbacher, and S. Köster, Biochim. Biophys. Acta **1853**, 3053 (2015).
[5] B. Eckes, D. Dogic, E. Colucci-Guyon, N. Wang, A. Maniotis, D. Ingber, A. Merckling, F. Langa, M. Aumailley, A. Delouvee *et al.*, J. Cell Sci. **111**, 1897 (1998).
[6] L. Ramms, G. Fabris, R. Windoffer, N. Schwarz, R. Springer, C. Zhou, J. Lazar, S. Stiefel, N. Hersch, U. Schnakenberg *et al.*, Proc. Natl. Acad. Sci. U.S.A. **110**, 18513 (2013).
[7] K. Seltmann, A. W. Fritsch, J. A. Käs, and T. M. Magin, Proc. Natl. Acad. Sci. U.S.A. **110**, 18507 (2013).
[8] M. J. C. Hendrix, E. A. Seftor, Y.-W. Chu, K. T. Trevor, and R. E. B. Seftor, Cancer Metastasis Rev. **15**, 507 (1996).
[9] C. Leduc and S. Etienne-Manneville, Curr. Opin. Cell Biol. C **32**, 102 (2015).
[10] Y. Messica, A. Laser-Azogui, T. Volberg, Y. Elisha, K. Lysakovskaia, R. Eils, E. Gladilin, B. Geiger, and R. Beck, Nano Lett. **17**, 6941 (2017).
[11] L. Kreplak, H. Bär, J. F. Leterrier, H. Herrmann, and U. Aebi, J. Mol. Biol. **354**, 569 (2005).
[12] L. Kreplak, H. Herrmann, and U. Aebi, Biophys. J. **94**, 2790 (2008).
[13] J. Block, H. Witt, A. Candelli, E. J. G. Peterman, G. J. L. Wuite, A. Janshoff, and S. Köster, Phys. Rev. Lett. **118**, 048101 (2017).
[14] B. Nöding and S. Köster, Phys. Rev. Lett. **108**, 088101 (2012).
[15] N. Mücke, L. Kreplak, R. Kirmse, T. Wedig, H. Herrmann, U. Aebi, and J. Langowski, J. Mol. Biol. **335**, 1241 (2004).
[16] J. Block, V. Schroeder, P. Pawelzyk, N. Willenbacher, and S. Köster, Biochim. Biophys. Acta Mol. Cell Res. **1853**, 3053 (2015).
[17] J. Block, H. Witt, A. Candelli, J. C. Danes, E. J. G. Peterman, G. J. L. Wuite, A. Janshoff, and S. Köster, Sci. Adv. **4**, eaat1161 (2018).
[18] D. S. Fudge, K. H. Gardner, V. T. Forsyth, C. Riekel, and J. M. Gosline, Biophys. J. **85**, 2015 (2003).
[19] J. Cao and C. A. Billows, Polym. Int. **48**, 1027 (1999).
[20] L. Kreplak, J. Doucet, P. Dumas, and F. Briki, Biophys. J. **87**, 640 (2004).
[21] Z. Qin, L. Kreplak, and M. J. Buehler, PLoS One **4**, e7294 (2009).
[22] H. Herrmann, M. Häner, M. Brettel, S. A. Müller, K. N. Goldie, B. Fedtke, A. Lustig, W. W. Franke, and U. Aebi, J. Mol. Biol. **264**, 933 (1996).
[23] E. G. Bendit, Text. Res. J. **30**, 547 (1960).
[24] J. Forsting, J. Kraxner, H. Witt, A. Janshoff, and S. Köster, Nano Lett. **19**, 7349 (2019).
[25] H. Herrmann, L. Kreplak, and U. Aebi, Methods Cell Biol. **78**, 3 (2004).
[26] See Supplemental Material at http://link.aps.org/supplemental/10.1103/PhysRevLett.123.188102 for details of the protein preparation, data analysis, theoretical model and further comments.
[27] W. H. Moolenaar, L. G. Tertoolen, and S. W. de Laat, Nature **312**, 371 (1984).
[28] G. Bright, G. Fisher, J. Rogowska, and D. Taylor, J. Cell Biol. **104**, 1019 (1987).
[29] I. H. Madshus, Biochem. J. **250**, 1 (1988).
[30] P. A. Coulombe and E. Fuchs, J. Cell Biol. **111**, 153 (1990).
[31] H. Herrmann, T. Wedig, R. M. Porter, E. B. Lane, and U. Aebi, J. Struct. Biol. **137**, 82 (2002).
[32] N. Mücke, T. Wedig, A. Bürer, L. N. Marekov, P. M. Steinert, J. Langowski, U. Aebi, and H. Herrmann, J. Mol. Biol. **340**, 97 (2004).
[33] R. H. Kretsinger, V. Uversky, and E. Permyakov, *Encyclopedia of Metalloproteins* (Springer, New York, 2013).
[34] M. Zacchia, M. L. Abategiovanni, S. Stratigis, and G. Capasso, Kidney disease **2**, 72 (2016).
[35] R. Janissen, B. A. Berghuis, D. Dulin, M. Wink, T. Van Laar, and N. H. Dekker, Nucleic Acids Res. **42**, e137 (2014).
[36] Z. Qin and M. J. Buehler, J. Mol. Model. **17**, 37 (2011).
[37] T. Ackbarow and M. J. Buehler, Nanotechnology **20**, 075103 (2009).
[38] C. Dammann and S. Köster, Lab Chip **14**, 2681 (2014).
[39] C. Y. J. Hémonnot, M. Mauermann, H. Herrmann, and S. Köster, Biomacromolecules **16**, 3313 (2015).
[40] J. Kyte and R. F. Doolittle, J. Mol. Biol. **157**, 105 (1982).
[41] S. Nafeey, I. Martin, T. Felder, P. Walther, and E. Felder, J. Struct. Biol. **194**, 415 (2016).
[42] G. Bell, Science **200**, 618 (1978).

[43] T. Erdmann and U. S. Schwarz, Phys. Rev. Lett. **92**, 108102 (2004).
[44] U. Aebi, W. E. Fowler, P. Rew, and T. T. Sun, J. Cell Biol. **97**, 1131 (1983).
[45] D. A. Parry, L. N. Marekov, and P. M. Steinert, J. Biol. Chem. **276**, 39253 (2001).
[46] L. Kreplak, A. Franbourg, F. Briki, F. Leroy, D. Dalle, and J. Doucet, Biophys. J. **82**, 2265 (2002).
[47] K. N. Goldie, T. Wedig, A. K. Mitra, U. Aebi, H. Herrmann, and A. Hoenger, J. Struct. Biol. **158**, 378 (2007).
[48] A. Kolomeisky, *Motor Proteins and Molecular Motors* (CRC Press, Boca Raton, 2015).
[49] M. E. Fisher and A. B. Kolomeisky, Proc. Natl. Acad. Sci. U.S.A. **96**, 6597 (1999).
[50] See Supplemental Material [26] for further mechanical characterization of the model, which includes Ref. [51].
[51] U. Seifert, Phys. Rev. Lett. **84**, 2750 (2000).
[52] D. J. Tobias, S. F. Sneddon, and C. L. Brooks, J. Mol. Biol. **227**, 1244 (1992).
[53] A.-S. Yang and B. Honig, J. Mol. Biol. **252**, 366 (1995).
[54] S. Singh, C.-c. Chiu, A. S. Reddy, and J. J. de Pablo, J. Chem. Phys. **138**, 155101 (2013).
[55] M. Rief, J. Pascual, M. Saraste, and H. E. Gaub, J. Mol. Biol. **286**, 553 (1999).
[56] H. Takahashi, F. Rico, C. Chipot, and S. Scheuring, ACS Nano **12**, 2719 (2018).
[57] S. Winheim, A. R. Hieb, M. Silbermann, E.-M. Surmann, T. Wedig, H. Herrmann, J. Langowski, and N. Mücke, PLoS One **6**, e19202 (2011).
[58] A. Premchandar, N. Mücke, J. Poznański, T. Wedig, M. Kaus-Drobek, H. Herrmann, and M. Dadlez, J. Biol. Chem. **291**, 24931 (2016).
[59] A. Premchandar, A. Kupniewska, K. Tarnowski, N. Mücke, M. Mauermann, M. Kaus-Drobek, A. Edelman, H. Herrmann, and M. Dadlez, J. Struct. Biol. **192**, 426 (2015).
[60] T. Lichtenstern, N. Mücke, U. Aebi, M. Mauermann, and H. Herrmann, J. Struct. Biol. **177**, 54 (2012).
[61] Human intermediate filament database, http://www.interfil.org (accessed 2019).
[62] C. Dammann, B. Nöding, and S. Köster, Biomicrofluidics **6**, 022009 (2012).
[63] C. Dammann, H. Herrmann, and S. Köster, Isr. J. Chem. **56**, 614 (2016).